# Crossover among structural motifs in transition and noble-metal clusters

F. Baletto[a] and R. Ferrando[b]
*INFM and CFSBT/CNR, Dipartimento di Fisica dell'Università di Genova, via Dodecaneso 33, 16146 Genova, Italy*

A. Fortunelli[c]
*Istituto per i Processi Chimico-Fisici del CNR, Via V. Alfieri 1, 56124, Pisa, Italy*

F. Montalenti[d]
*Theoretical Division, Los Alamos National Laboratory, Los Alamos, New Mexico 87545*

C. Mottet[e]
*CRMC2/CNRS, Campus de Luminy, Case 913, 13288 Marseille Cedex 9, France*

(Received 25 October 2001; accepted 13 December 2001)

The energetics of nanoclusters is investigated for five different metals (Ag, Cu, Au, Pd, and Pt) by means of quenched molecular dynamics simulations. Results are obtained for two different semiempirical potentials. Three different structural motifs are considered: icosahedra (Ih), decahedra (Dh), and truncated octahedra (TO). The crossover sizes among structural motifs are directly calculated, considering cluster up to sizes $N \simeq 40\,000$. For all the systems considered, it is found that icosahedra are favored at small sizes, decahedra at intermediate sizes, and truncated octahedra at large sizes. However, the crossover sizes depend strongly on the metal: in Cu, the icosahedral interval is rather large, and it is followed by a very wide decahedral window; on the contrary, in Au, the icosahedral interval is practically absent, and the decahedral window is narrow. The other metals display intermediate behaviors, Ag being close to Cu, and Pd and Pt being close to Au. A simple criterion, which is based on the ratio between the bulk modulus and the cohesive energy per atom, is developed to account for the differences among the metals. © *2002 American Institute of Physics.* [DOI: 10.1063/1.1448484]

## I. INTRODUCTION

Clusters provide a bridge between isolated atoms and bulk material, and, because of that, they can display unusual physical and chemical behaviors. The knowledge of the structure is the starting point to understand the peculiar characteristics of a cluster.[1,2] It is well known that nanometer-size clusters can present both crystalline (fcc for the elements that we shall consider in the following) and noncrystalline structures. The latter are very common at small sizes, and, in the case of noble and transition metals, they take the form of icosahedra (Ih) and of Marks truncated decahedra (*m*-Dh).[1–3] In Fig. 1, examples of Ih, Dh, and fcc clusters are shown. Icosahedra have a quasispherical shape and a close-packed surface with 20 distorted (111)-like facets.[1] The Ih structure is obtained by packing together twenty tetrahedra sharing a common vertex. This packing is possible only if the tetrahedra are distorted, and this causes the high internal strain of the structure. Icosahedra are thus expected to be favorable at small sizes, where the efficient minimization of the surface energy prevails over the strain contribution, which is proportional to the cluster volume. The decahedral structure is obtained by packing five tetrahedra so that they have a common edge. In this way, the surface is again close-packed, being formed by 10 (111)-like facets, but the resulting cluster shape is quite far form a spherical one. Better Dh structures can be obtained, however, by truncating the clusters. The Ino truncation[4] exposes five rectangular (100)-like facets. The latter facets are not close-packed, but the resulting shape is closer to a sphere. However, this is not usually the best decahedral shape, since the energetically costly (100) facets are rather large in the Ino Dh. A better solution to the problem of finding the best Dh structure was given by Marks,[5] who proposed further truncations, which are done in such a way to create (111)-like re-entrant facets. In this way, the cluster shape remains still close to a sphere, but smaller open (100)-like facets are exposed. From the point of view of the surface energy, icosahedra are still better for small clusters, but decahedra have less internal strain, and become more favorable than icosahedra at increasing sizes. Finally, fcc clusters are expected to be the most favorable in the macroscopic limit, because this is the bulk lattice symmetry for the metals considered in this paper. Fcc octahedra present only (111) facets, but are very far from the spherical shape. Truncated octahedra have a better surface/volume ratio, but expose large (100) facets. Therefore, fcc structures present a large surface energy, but they lack internal strain, and are thus expected to dominate at large sizes. These general trends are common to many fcc-bulk systems, ranging from metallic to Lennard-Jones clusters (as demonstrated by calculations[6–9] and

[a]Electronic mail: baletto@fisica.unige.it
[b]Author to whom correspondence should be addressed. Electronic mail: ferrando@fisica.unige.it
[c]Electronic mail: fortunelli@icqem.pi.cnr.it
[d]Electronic mail: montalenti@t12.lanl.gov
[e]Electronic mail: mottet@crmc2.univ-mrs.fr

 

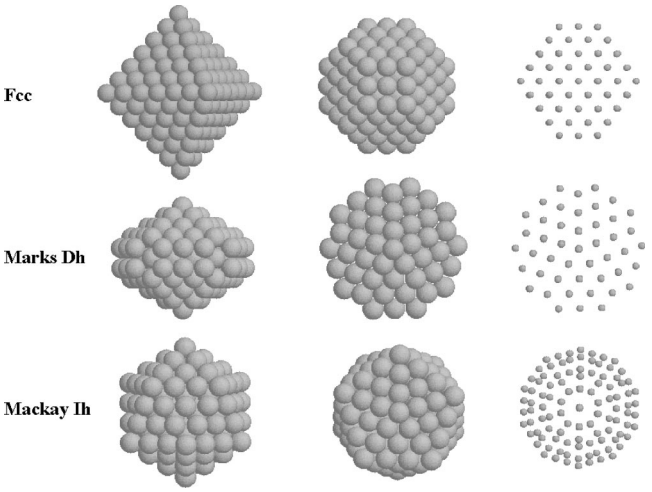


FIG. 1. Structural motifs of clusters. In the top row, at left a perfect octahedron is shown; in the middle panel and right panels, a truncated octahedron, obtaining truncating the six vertices of the octahedron, is shown. In the middle row, the (3,2,2) Marks decahedron is shown in different views. Note the rectangular (100)-like facets of size $3\times2$ ($m=3$, $n=2$), and the Marks re-entrance. In the bottom row, the fourth shell Icosahedron is shown in different views.

experiments[10,11]). We expect that they shall hold also for the metals treated in this paper, which are thus expected to show a crossover among structural motifs, from icosahedra, to decahedra and finally to fcc clusters. An interesting point is therefore to investigate quantitatively the crossover sizes for the different metals, looking at the best clusters for each structural motifs, and trying to devise general trends among the different elements and to give, if possible, some simple criteria for understanding *a priori* their behaviors. This is the purpose of the present paper, in which we shall treat explicitly Cu, Ag, Au, Pd, and Pt clusters. There are already several papers (see, for example Refs. 7, 8, 12, 13) dealing with crossover sizes in metallic clusters, but they either treat a single element (Ni in Ref. 7), or they are limited to rather small sizes, well below the crossover ones,[8] or they compare only Ih structures with cuboctahedra[13] [which are indeed very unfavorable fcc structures with large (100) facets] and truncated octahedra.[12] The present work synoptically treats several elements up to large sizes ($N\leqslant40\,000$), and searches for the best clusters for each structural motif.

The paper is structured as follows: in Sec. II we briefly describe the interaction potentials and the calculation method; in Sec. III we report the results of the energy minimization of the clusters for the three structural motifs comparing the five metals; Sec. IV develops a simple criterion to devise general trends among the different metals; Sec. V contains the conclusions.

## II. THE MODEL

As anticipated in the Introduction, we calculate cluster energies by two different semiempirical many-body potentials. The first one was proposed by Rosato, Guillopè, and Legrand (RGL).[14,15] Then we check general trends by comparing with the results of an embedded atom method (EAM) potential[16] as parametrized by Voter.[17,18] The RGL potential has a very simple analytical expression depending on five parameters, and because of that, it is well suited for discussing general trends and for comparing the different metals in a rather easy way. In the following, we give a brief description of the RGL potential; for the EAM potential we refer to the original literature.[18] In the RGL potential, the cohesion of the crystal is given by an attractive many-body term (the band energy), which for an atom $i$ is given by

$$E_b^i=-\left\{\sum_{j,r_{ij}<r_c}\xi^2\exp\left[-\frac{q}{\alpha}\left(\frac{r_{ij}}{r_0}-1\right)\right]\right\}^{\alpha}; \tag{1}$$

$\alpha=1/2$ in the second-moment approximation to the tight-binding model;[14] other exponents have been proposed in the literature.[13,19] The stability of the cluster is ensured by adding a phenomenological core-repulsion term $E_b^r$ of the Born–Mayer-type,

$$E_r^i=\sum_{j,r_{ij}<r_c}A\exp\left[-p\left(\frac{r_{ij}}{r_0}-1\right)\right]. \tag{2}$$

In these expressions, $r_{ij}$ is the distance between atoms $i$ and $j$, $r_c$ is the cutoff radius of the interactions (in the following calculations, we use the above form of the potential up to the second-neighbor distance, and link smoothly the potential to zero at the third-neighbor distance); $r_0$ is the nearest-neighbor distance in the bulk; $A$, $\xi$, $p$, $q$ are parameters fitted on bulk properties of the metals, i.e., the cohesive energy, the bulk modulus and the annihilation of the energy gradient at $r_0$. Their values are given in Table I. It can be noted that, after fitting the bulk properties, one is left with only two independent parameters, say, $p$ and $q$. $p$ and $q$ determine the range of the repulsive and of the attractive part of the potential, respectively; as we shall see in Sec. IV, these two parameters define the trends among the different metals.

TABLE I. Lattice constant $a$ and RGL parameters for the different metals.

| Metal | $a=\sqrt{(2)}r_0$ (Å) | $\xi$ (eV) | $A$ (eV) | $p$ | $q$ |
|---|---|---|---|---|---|
| Cu | 3.62 | 1.280 | 0.0894 | 10.55 | 2.43 |
| Ag | 4.09 | 1.190 | 0.1031 | 10.85 | 3.18 |
| Au | 4.07 | 1.855 | 0.2197 | 10.53 | 4.30 |
| Pd | 3.89 | 1.702 | 0.1715 | 11.00 | 3.79 |
| Pt | 3.92 | 2.621 | 0.2477 | 10.71 | 3.85 |

The cohesive energy of a cluster of atoms is given by

$$E_c=\sum_i\,(E_b^i+E_r^i). \tag{3}$$

Detailed comparisons of RGL results for diffusion barriers on flat and stepped surfaces with experimental data, *ab initio*, and semiempirical calculations are reported in Ref. 20. It turns out that RGL results correctly predict the dominant diffusion mechanisms on noble and transition metal surfaces;[21,22] from the quantitative point of view, the agreement with experimental data and first-principle calculations is usually good, especially for silver. Moreover, the use of these potentials in the modeling of silver clusters growth[23,24] has lead to the explanation of the experimental phenomenology.[25]

Comparison with density functional calculations for noble-metal clusters are reported in Ref. 26, where once again a good agreement is found.

In the following, the total energy of the clusters is calculated by quenched molecular dynamics, which allows the complete relaxation of the structures around a local minimum. At the sizes which will be considered in the following, global optimization[27] is not feasible.

## III. RESULTS

Here we report the results concerning the different structural motifs for the metals Ag, Au, Cu, Pd, and Pt. We report a thorough study of the energetics of the different structural motifs by RGL potentials, considering large clusters and determining crossover sizes. Then we check the general trends about the transition from icosahedra and decahedra by means of the EAM potentials. Ag is treated in greater details as a reference case.

Before showing the results we introduce few notations and indices related to the different structures, in order to facilitate their geometrical description, and we introduce the quantity $\Delta$ (see below), which is useful to discuss the relative stability of structures of different sizes.

*Icosahedra*: They are structured in shells, see Fig. 1. An Ih with $k$ shells has

$$N_{\mathrm{Ih}}(k)=\frac{10}{3}k^3-5k^2+\frac{11}{3}k-1 \tag{4}$$

atoms (so that the series of magic numbers is 1, 13, 55, 147,...) and presents 20 triangular facets of side $k$.

*Marks decahera*: They are characterized by three indices $(m, n, r)$ (in previous works,[23,24] the third index was named $p$ instead of $r$, but here that choice would lead to a confusing notation because of the parameter $p$ of the RGL potential). $m$ and $n$ are the length of the sides of the (100) facets, perpendicular and parallel to the fivefold axis, respectively (see Fig. 1); $r$ is the depth of the Marks re-entrance ($r=1$ corresponds to no re-entrance i.e., to the Ino decahedron). A $(m, n, r)$ marks Dh has $h=m+n+2r-3$ atoms along its symmetry axis and a total number of atoms $N_{\mathrm{Dh}}(m,n,r)$ given by

$$\begin{aligned}N_{\mathrm{Dh}}(m,n,r)=\tfrac{1}{6}\{&30r^3-135r^2+207r-102+[5m^3\\&+(30r-45)m^2+(60(r^2-3r)\\&+136)m]+n[15m^2+(60r-75)m\\&+3(10r^2-30r)+66]\}-1.\end{aligned} \tag{5}$$

*fcc polyhedra*: Starting from the octahedron (see Fig. 1), better fcc polyhedra are obtained truncating symmetrically the six vertices, thus obtaining square and hexagonal (triangular in the case of cuboctahedra) facets. In the following we characterize a given truncated octahedron (TO) by two indexes: $n_l$ is the length of the edge of the complete octahedron; $n_{\mathrm{cut}}$ is the number of layers cut at each vertex. A TO has a number of atoms,

$$N_{\mathrm{TO}}(n_l,n_{\mathrm{cut}})=\tfrac{1}{3}(2n_l^3+n_l)-2n_{\mathrm{cut}}^3-3n_{\mathrm{cut}}^2-n_{\mathrm{cut}}, \tag{6}$$

and square facets with edges of $n_{\mathrm{cut}}+1$ atoms. Concerning the (111) hexagonal facets, they are not in general regular hexagons. In fact, three edges of the hexagons are in common with square facets, having thus $n_{\mathrm{cut}}+1$ atoms, while the remaining three edges have $n_l-2n_{\mathrm{cut}}$ atoms. Regular hexagons are thus possible if $n_l=3n_{\mathrm{cut}}+1$; in the following the TO with regular hexagonal facets will be referred to as regular TO. On the other hand, cuboctahedra are characterized by $n_l=2n_{\mathrm{cut}}+1$, which gives energetically unfavorable clusters with large (100) facets and triangular (111) facets; by substituting this relation into Eq. (6), and comparing with Eq. (4), one finds that a cuboctahedron with a given $n_{\mathrm{cut}}$ has the same number of atoms as an Ih with $k=n_{\mathrm{cut}}+1$.

The quantity, which we introduce to compare the energetics of clusters of different sizes $N$, is $\Delta$,[3,7,8] defined as

$$\Delta=\frac{E_{\mathrm{tot}}-NE_{\mathrm{coh}}}{N^{2/3}}, \tag{7}$$

where $E_{\mathrm{tot}}$ is the total energy of the cluster after the relaxation of the structure and $E_{\mathrm{coh}}$ is the cohesive energy per atom in the bulk. $\Delta$ is thus the excess energy roughly divided by the number of surface atoms. In general, we expect the following expression to hold for $\Delta$:[7,8]

$$\Delta=\frac{a+bN^{1/3}+cN^{2/3}+dN}{N^{2/3}}. \tag{8}$$

In the numerator (which is the excess energy), the constant comes from the vertices of the cluster, the term in $N^{1/3}$ from the edges, the term in $N^{2/3}$ from the facets, and the volume term in $N$ is due to the internal strain. This last term is always present in Ih and Dh clusters, while in TO vanishes (at least in the limit of large sizes). Therefore, for TO clusters, $\Delta$ decreases with size and tends to a constant at $N\to\infty$, while for Ih and Dh $\Delta$ initially decreases, then reaches a minimum, and finally diverges at large sizes as $N^{1/3}$.

### A. Ag clusters

*Icosahedra*: Silver icosahedra decrease their $\Delta$ up to $N=147$ (fourth shell Ih) according to the RGL potential (see Fig. 2).

*Decahedra*: The best Ag decahedra have $m=n$, which gives square (100) facets, and a more spherical cluster shape. Concerning the Marks reentrance, the best clusters have $r\simeq m/2$. As we shall see in the following, while the choice $m=n$ is common to all the metals treated here, the choice of $r$ changes with the metal, and relative trends can be understood comparing the surface energies of the (100) and (111) surfaces [$\gamma_{(100)}$ and $\gamma_{(111)}$ respectively]. Indeed, increasing $r$, the proportion of (111) facets increases, and thus metals characterized by larger ratios $\gamma_{(100)}/\gamma_{(111)}$ (see Table II) prefer larger $r$ than $m/2$. Once the sequence of the best decahedra is chosen ($m=n$, $r\simeq m/2$), $\Delta$ decreases up to sizes $N\simeq 15\,000$ for RGL potentials [where the best clusters are the (10, 10, 5) and the (10, 10, 6) Dh, at $N=10\,887$ and $N=13\,829$, respectively], and it decreases at least up to 1000 atoms for the EAM potential. According to RGL potentials, decahedra are the best structures in the interval $300<N<20\,000$.

*fcc clusters*: A criterion which can be helpful in finding the best TO structures is the Wulff construction (see, for example, Ref. 28), which was indeed developed to find the

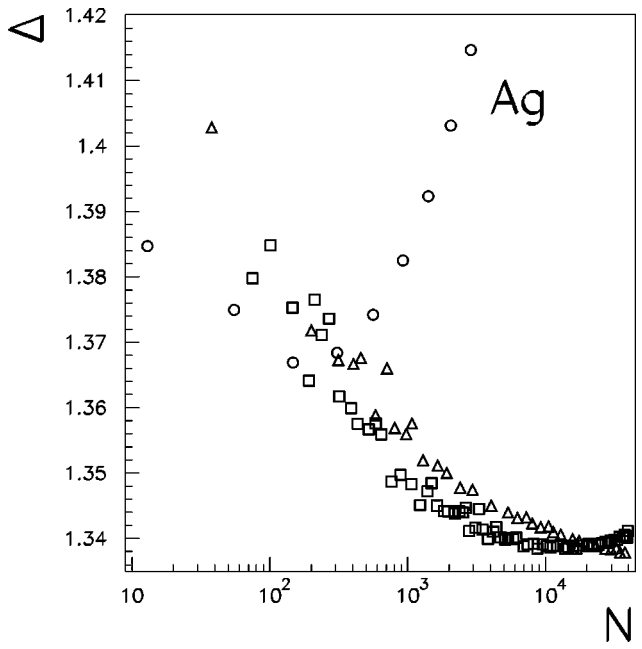


FIG. 2. The quantity $\Delta=(E_{\mathrm{tot}}-NE_{\mathrm{coh}})/N^{2/3}$ as a function of the size $N$, calculated by means of RGL potentials for silver clusters. Circles, squares, and triangles refer to icosahedra, decahedra, and truncated octahedra, respectively.

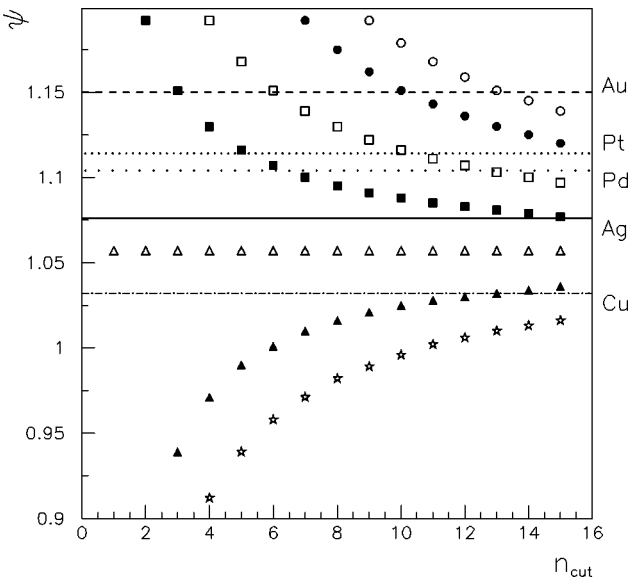


FIG. 3. Ratio $\psi=d_{(100)}/d_{(111)}$ as a function of $n_{\mathrm{cut}}$ for different series of truncated octahedra (TO). Each series is represented by different symbols: the open circles are related to TO structures with $n_l=3n_{\mathrm{cut}}+4$, the full circles to TO with $n_l=3n_{\mathrm{cut}}+3$, the open squares to TO with $n_l=3n_{\mathrm{cut}}+2$, the full squares to regular TO having $n_l=3n_{\mathrm{cut}}+1$, the open triangles to TO with $n_l=3n_{\mathrm{cut}}$, the full triangles to TO with $n_l=3n_{\mathrm{cut}}-1$, and the stars to TO with $n_l=3n_{\mathrm{cut}}-2$. The horizontal lines represent the ratio of surface energies $\gamma_{(100)}/\gamma_{(111)}$ for the five metals.

equilibrium shape of macroscopic crystals by the minimization of the surface energy for a crystal of a given volume. From the Wulff construction, the best TO structure should fulfill the following condition:

$$\frac{\gamma_{(100)}}{\gamma_{(111)}}=\frac{d_{(100)}}{d_{(111)}}, \tag{9}$$

where $\gamma_{(100)}$ and $\gamma_{(111)}$ are the (100) and (111) surface energies, respectively, whereas $d_{(100)}$ and $d_{(111)}$ are the distances from the center of the cluster. In Fig. 3, we report the ratio $\psi=d_{(100)}/d_{(111)}$ for the most significant unrelaxed TO structures in the nanometric size range, compared to the ratio of the surface energies for the different metals. The energy relaxation shows that either regular TO [characterized by $n_{\mathrm{cut}}^R$ and $n_l^R=3n_{\mathrm{cut}}^R+1$, see Fig. 3] or TO with slightly larger (100) facets than the regular TO (say with $n_l=n_l^R-1$ and $n_{\mathrm{cut}}=n_{\mathrm{cut}}^R$, which gives $n_l=3n_{\mathrm{cut}}$) are the most favorable at sufficiently large size, in good agreement with the Wulff construction criterion (compare the ratio of the surface energies in Table II with the data in Fig. 3), which turns out to be useful also for nanometer-size objects in the case of silver.

TABLE II. Ratio between the relaxed surface energies of (100) and (111) faces in the case of RGL potentials with $\alpha=\frac{1}{2}$.

| Metal | $\gamma_{(100)}/\gamma_{(111)}$ |
|---|---|
| Cu | 1.032 |
| Ag | 1.076 |
| Pd | 1.104 |
| Pt | 1.114 |
| Au | 1.150 |

### B. Other metals

In this section, we treat Cu, Au, Pd, and Pt clusters. Our results are reported in Fig. 4 using the RGL potential and in Fig. 5 for the EAM. In the latter case we consider a smaller size range ($N\simeq 1000$) just to analyze the crossover between icosahedra and decahedra. In the following we report in detail the results obtained with RGL potentials.

We find that the size interval in which a kind of structure is favored depends strongly on the metal. So we can find copper clusters which present icosahedral structures up to 1000 atoms and a very great size interval for decahedra (the crossover with fcc is at $N>30\,000$), while gold clusters prefer fcc structures already at sizes larger than 600 atoms. An intermediate behavior characterizes Pt and Pd clusters. In fact, for these metals, we find that icosahedra are favored only at very small sizes and the crossover between Dh and fcc is at $N\sim 6000-7000$ atoms.

Moreover, we find that the best choices for $(m, n, r)$ for decahedra and $n_l$ and $n_{\mathrm{cut}}$ for TO structures depend on metals. In the case of decahedral structures the choice $m=n$ is common to all metals, because in this way the cluster is much more spherical, while $r$ is much larger in the case of Au clusters for which we have $r=m$ [the best Dh is the (3,3,3) at 433 atoms] than for Cu [decahedra decrease their $\Delta$ up to (10,10,5) at 10 887 atoms] and Ag clusters where $r\simeq m/2$. This means that Au clusters prefer to have deep reentrances or in other words, large (111) facets [remember that for gold a (111) facet presents a much better surface energy than a (100) facet (see Table II)]. Again Pt and Pd clusters present an intermediate choice: at small sizes $r\simeq m$ and at larger sizes $r=m-2$ or $r=m-3$ [for both metals the minimum is the (7,7,5) Dh at 5341 atoms].

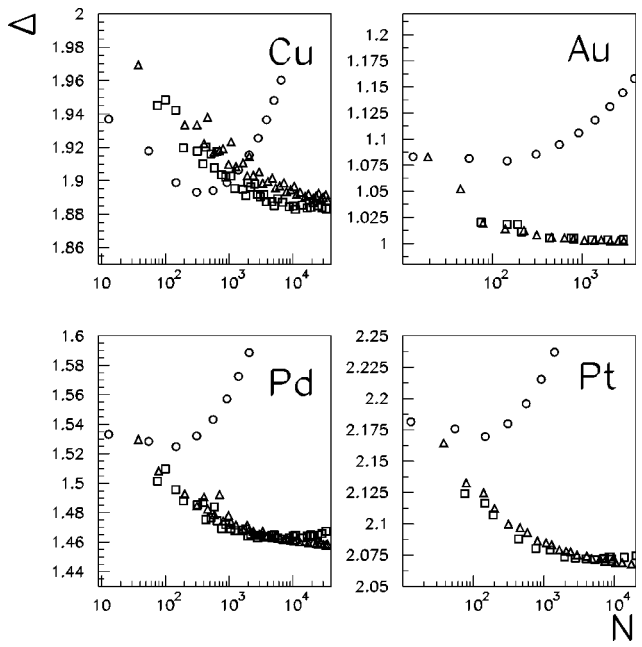


FIG. 4. Δ calculated by RGL potentials for Cu, Au, Pd, and Pt clusters. Symbols as in Fig. 2.

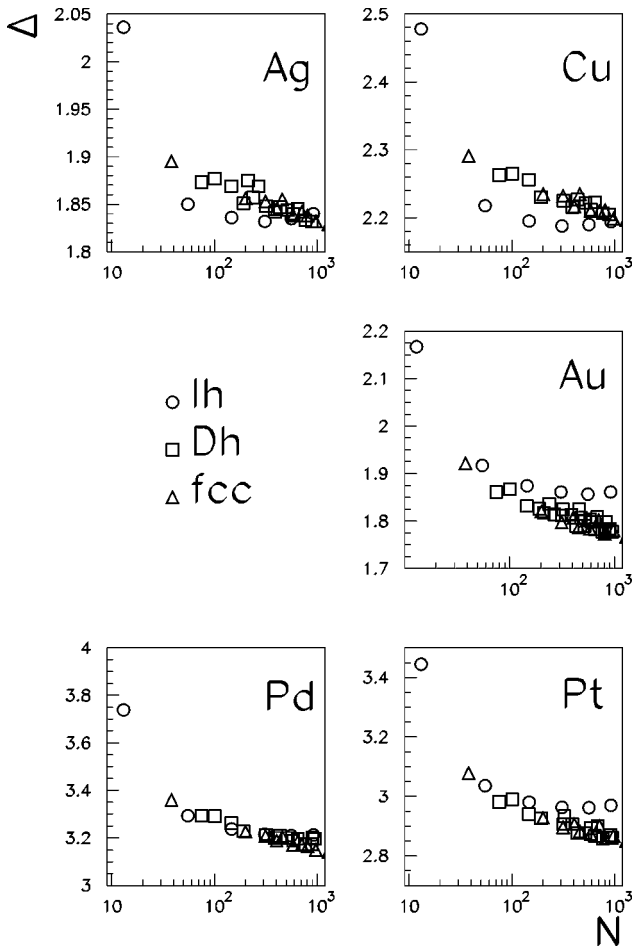


FIG. 5. Δ calculated by EAM potentials for Ag, Cu, Au, Pd, and Pt clusters. Symbols as in Fig. 2.

The best choice of $n_l$ and $n_{\mathrm{cut}}$ satisfies generally the Wulff construction, especially when the cluster is not too small, as can be understood by the comparison of Table II and Fig. 3. Again we find that gold clusters are characterized by large hexagonal (111) facets (the best TO structures are characterized by $n_l=3n_{\mathrm{cut}}+3$ at small sizes and $n_l=3n_{\mathrm{cut}}+4$ at larger sizes) while Pt and Pd prefer $n_l=3n_{\mathrm{cut}}+2$ (for large Pt clusters also the choice $n_l=3n_{\mathrm{cut}}+3$ is very good), and Cu fcc clusters are characterized by $n_l=3n_{\mathrm{cut}}$. We remember that for Ag clusters we have regular TO, with $n_l=3n_{\mathrm{cut}}+1$. These results are in very good agreement with the ratio $\gamma_{100}/\gamma_{111}$ reported in Table II: in fact, we find that Cu and Ag, which present the lowest ratio, prefer smaller (111) facets than Au, which has the largest ratio.

Finally, we remark that, in the case of gold, it is known from literature[26] that, at small sizes, amorphous structures may play an important role. We do not consider them because the principal aim of our work is to make a comparison between different metals trying to find a simple method to devise *a priori* general trends about the crossover sizes between different structural motifs, whereas amorphous structures are favorable only for gold and maybe for platinum clusters.

### C. Comparison of RGL and EAM results

Here we compare the results of the two potentials at sizes $N<1000$ (see Figs. 2, 4, 5). First of all, we notice that for each metal, the values of Δ obtained by the two potentials are rather different. However, the values in themselves are not of great importance. For example, we have made the following check. We have calculated Δ by means of a second parametrization of the RGL potential (the one in Ref. 15) which differs from the one used in Figs. 2 and 4 essentially because the cutoff distance for the interactions is larger. In that case, the curves of $\Delta(N)$ are shifted to higher values, but crossover sizes remain unaltered.

If we compare crossover sizes for the transition Ih $\rightarrow$Dh, we see that RGL results are in agreement with the EAM results from a qualitative viewpoint. In fact, also in this case we find that copper clusters present a broad size window in which Ih are the best structures (Δ decreases up to 309 atoms and the crossover with decahedra is at $N>1000$), which is followed by a large decahedral interval, while gold disfavors this kind of structures and prefers the fcc shape already at small sizes: there is a strong competition between Dh and fcc already at $N\simeq 400$. Silver has an intermediate behavior (closer to Cu than to Au) also according to EAM potentials, while Pt is closer to Au.

In conclusion, the major difference between RGL and EAM results is that, within the EAM potential description, palladium clusters present a behavior much more similar to Ag than to Pt (the icosahedral interval is wider: Ih are the best up to 150 atoms).

## IV. DISCUSSION

In this section, we try to develop a simple criterion for explaining the trends shown by the different metals about the crossover sizes. Due to their rather simple analytical form,

TABLE III. Parameter $\sigma=\rho(\varepsilon)/\varepsilon^2$ in the cases of first ($\sigma_{1n}=pq/2$) and second neighbor ($\sigma_{2n}$, see Appendix for the formula) cutoff, sizes where $\Delta$ is minimum ($N_\Delta^{\mathrm{Ih}}$ for icosahedra and $N_\Delta^{\mathrm{Dh}}$ for decahedra), and crossover sizes ($N_{\mathrm{Ih}\to\mathrm{Dh}}$ and $N_{\mathrm{Dh}\to\mathrm{fcc}}$), in the case of the different metals and for the RGL potentials.

| Metal | $\sigma_{1n}$ | $\sigma_{2n}$ | $N_\Delta^{\mathrm{Ih}}$ | $N_\Delta^{\mathrm{Dh}}$ | $N_{\mathrm{Ih}\to\mathrm{Dh}}$ | $N_{\mathrm{Dh}\to\mathrm{fcc}}$ | $N_{\mathrm{Ih}\to\mathrm{fcc}}$ |
|---|---|---|---|---|---|---|---|
| Cu | 13.1 | 14.4 | 309 | 20000 | 1000 | >30000 | 1500 |
| Ag | 17.2 | 18.3 | 147 | 14000 | <300 | 20000 | 400 |
| Pd | 20.9 | 21.8 | 147 | 5300 | <100 | 6500 | <100 |
| Pt | 20.6 | 21.5 | 147 | 5300 | <100 | 6500 | <100 |
| Au | 22.6 | 23.3 | 147 | 1300 | <100 | 500 | <100 |

RGL potentials are well suited to discuss general trends as functions of the potential parameters. An example is the $(1\times2)$ missing-row reconstruction. This reconstruction is adopted by Ir, Pt, and Au(110) surfaces (the $5d$ series, while the $3d$ and $4d$ series do not reconstruct) and it has been theoretically ascribed[29] to the increase of the parameter $q$, which governs the attractive interaction dependence with distance, when going from $3d$ to $5d$ metals. Such an increase in $q$ for the fcc transition metals is consistent with the universal nature of binding-energy-distance relations.[30,31] A similar trend has been pointed out along the noble metal column concerning the vacancy stabilization in icosahedra.[12]

The question that we shall try to answer in the following is: Why are crossover sizes small for gold and large for copper? First of all, we notice that noncrystalline structures are distorted: even in the unrelaxed structure, nearest-neighbor atoms are placed at distances which are different from the nearest-neighbor distance in the bulk solid. Therefore, we expect that a crystal which increases strongly its energy for a change in interatomic distances (i.e., which has a ''sticky'' interatomic potential), would have small crossover sizes.[32] On the contrary, elements with less sticky interactions would have larger crossover sizes. Following this idea, we look for the effect on the total energy of a bulk crystal of changing all the interatomic distances by a factor, say

$$r_{ij}\to(1+\varepsilon)r_{ij}\,. \tag{10}$$

Then we develop the crystal energy per atom $E_i(\varepsilon)$ to the second order and divide it by the equilibrium value $|E_i(0)|$. We expect that the larger is the ratio,

$$\rho(\varepsilon)=\frac{E_i(\varepsilon)-E_i(0)}{|E_i(0)|}, \tag{11}$$

the smaller are the crossover sizes from icosahedra to decahedra and then from decahedra to fcc crystallites. $\rho(\varepsilon)$ is essentially the ratio between the bulk modulus and the cohesive energy per atom of the bulk crystal.

Let us now calculate $E_i(\varepsilon)$, and try to find a simple expression in terms of the parameters of the potential. We assume, for the moment, that interatomic interactions extend to first neighbors only. The inclusion of second neighbors introduces only minor changes (see the following). For first-neighbor interactions, we obtain [see Eqs. (1) and (2) with $\alpha=1/2$]:

$$\begin{aligned}E_i(\varepsilon)&=12A\exp(-p\varepsilon)-\sqrt{12}\xi\exp(-q\varepsilon)\\&\simeq12A-\sqrt{12}\xi-(12Ap-\sqrt{12}\xi q)\varepsilon\\&\quad+(6Ap^2-\sqrt{3}\xi q^2)\varepsilon^2.\end{aligned} \tag{12}$$

The first-order term is zero because of the equilibrium condition on the crystal; this gives

$$\sqrt{12}Ap=\xi q, \tag{13}$$

and therefore

$$\rho(\varepsilon)=\tfrac{1}{2}pq\varepsilon^2. \tag{14}$$

From the above arguments, this result would indicate that *the larger is pq, the smaller are the crossover sizes*. This is indeed the case, as can be seen in Table III, where also results for second-neighbor interactions are reported. In the latter case one finds again $\rho(\varepsilon)=f(p,q)\varepsilon^2$, with $f(p,q)$ of a rather complicated form (see the Appendix); however, the inclusion of second neighbors does not introduce significant changes. A simple interpretation to Eq. (14) follows from the fact that $p$ and $q$ determine the range of the repulsive and of the attractive parts of the potential, respectively [see Eqs. (1) and (2)]; smaller $p$ and $q$ give a longer range (and less sticky) potential. We can notice from Table I that, whereas $p$ does not vary monotonically, $q$ increases from $3d$ to $5d$ series as expected from the universal features of bonding in metals[30,31] so that $pq$ is globally increasing from Cu to Au.

An equivalent way to correlate the metal-dependence of the stability domain of icosahedra relative to fcc-type structures with respect to the potential parameters is to give an analytical expression of the energies involved in the most simple cases: the 13 atoms clusters with icosahedral or cuboctahedral (TO with $n_l=2n_{\mathrm{cut}}+1$ and same atoms number as the Ih) symmetry. In these cases, the relaxed structures display only three different interatomic distances: one radial ($r_1$) and one tangential ($r_2$) for $\mathrm{Ih}_{13}$, and only one ($r_3$) for

TABLE IV. Interatomic radial ($r_1$) and tangential ($r_2$) distances in the $\mathrm{Ih}_{13}$ and the one ($r_3$) in the $\mathrm{TO}_{13}$ after relaxation versus the equilibrium distance in the bulk ($r_0$).

| Metal | $\frac{r_1}{r_0}$ | $\frac{r_2}{r_0}$ | $\frac{r_3}{r_0}$ |
|---|---|---|---|
| Cu | 0.928 | 0.976 | 0.950 |
| Ag | 0.924 | 0.972 | 0.945 |
| Au | 0.920 | 0.967 | 0.939 |

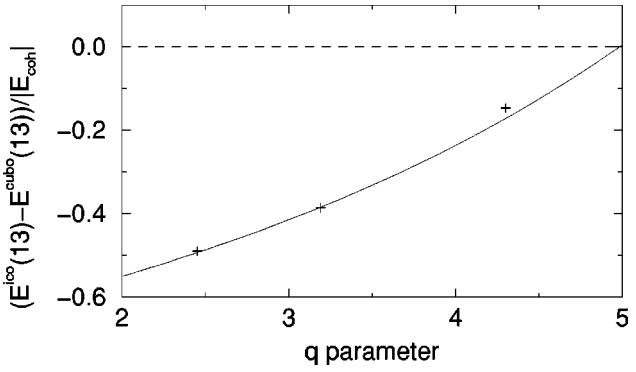


FIG. 6. Normalized energy difference between the Ih and the TO (cuboctahedron) of 13 atoms as a function of the parameter $q$.

the $TO_{13}$. If we note $P_i = e^{-p((r_i/r_0)-1)}$ and $Q_i = e^{-q((r_i/r_0)-1)}$ the distance dependencies of the repulsive and attractive terms of the potential, we can write the energy difference between $Ih_{13}$ and $TO_{13}$ normalized by the bulk cohesive energy as follows:

$$\frac{E_{Ih_{13}}-E_{TO_{13}}}{|E_{coh}|}=\frac{1}{p-q}\{-p[Q_1+2\sqrt{3Q_1^2+15Q_2^2} -(2\sqrt{15}+1)Q_3]+q(2P_1+5P_2-6P_3)\}. \tag{15}$$

The values of $r_1$, $r_2$, and $r_3$ are noted in the Table IV. For noble metals, we can notice from Tables III and IV that the $p$ parameter and the interatomic distances are not so different from one metal to another, so that we use averaged values to plot Eq. (15) as a function of $q$; essentially, since $p$ is not changing much, to look at variations in $pq$ or in $q$ is the same thing. We check in Fig. 6 that the points representing the ''exact'' values fit quite well the curve so that we get an evolution of the energy difference between $Ih_{13}$ and $TO_{13}$ which decreases appreciably when $q$ increases, i.e., from Cu to Au. That means that the Ih is the most favorable for Cu then for Ag and at last for Au clusters. In order to extend this analysis to bigger sizes to evaluate the crossover transition from noncrystalline (Ih) to crystalline (TO) clusters in noble metals, we have compared the surface energy gain and the core energy loss of the Ih relatively to TO with the same atoms number for three different sizes: 13, 561, and 2057 in order to distinguish the trend in the crossover transition from one metal to another. Looking at Table V we notice that except for the 13-atoms clusters where core defect is increasing from Cu to Au along the series, the core energy loss is quasi constant for the three metals and independent of the size [this is coherent with the divergence as $N^{1/3}$ of $\Delta$ at large sizes, see Eq. (8)], whereas the surface energy gain is decreasing from Cu to Au so that Cu Ih are more favorable (in a larger size range) than Ag and Au ones. This second analysis confirms the first one related to the stickiness of the potential[32] in order to predict the crossover size transition from $3d$ to $5d$ transition and noble metals series.

## V. SUMMARY AND CONCLUSIONS

In conclusion, we present a study of the energetics of five transition and noble metal clusters, and make a comparison among them trying to find simple ways to understand *a priori* general trends about crossover sizes among different structures.

We consider three structural motifs: icosahedra, truncated decahedra, and truncated octahedra for Cu, Ag, Au, Pd, and Pt.

We calculate the cluster energy by quenched molecular dynamics as a function of the cluster size $N$ and considering both the RGL and EAM potential. Moreover, in the case of Dh and fcc structures we find a criterion to determine the best choice of the parameters which identify the cluster shape: $(m, n, r)$ for decahedra and $n_l$ and $n_{cut}$ for TO. We find that their choice depends on metals according to the ratio $\gamma_{100}/\gamma_{111}$. In fact, we show that Au clusters, which present the largest ratio, prefer to have large (111) facet so they are characterized by $r=m$ and $n_l=3n_{cut}+3$. On the other hand, Cu and Ag clusters, which have the smallest ratio, present both $r=m/2$ and $n_l=3n_{cut}$, $n_l=3n_{cut}+1$, respectively. The best choice for Pd and Pt clusters is just in the middle: $r \simeq m-2$ and $n_l=3n_{cut}+2$.

Once we have found the best sequence for the three structural motifs, we can establish the crossover size among different structures and then make a comparison between metals. We demonstrate that copper and gold clusters have completely different behaviors. In fact, in the case of Cu clusters we find that non-crystalline structures are favored in wide intervals of size, while Au disfavors completely the icosahedral motif, with fcc clusters already at small sizes. The other metals present intermediate behaviors: silver is much more similar to copper while palladium and platinum are close to gold. The trends we find for different metals are in line with simple considerations based on the strain energy of the structures, due to the distortion of the interatomic distances in the noncrystalline structures. To estimate the effect of the strain on the excess energy, we introduce a small uniform expansion $\varepsilon$ in the interatomic distances of the fcc bulk crystal, and we develop the crystal energy per atom $E_i(\epsilon)$ to the second order, subtract the equilibrium value $E_i(0)$ and divide by $|E_i(0)|$, thus obtaining the quantity $\rho(\epsilon)$, which is essentially the bulk modulus divided by the cohesive energy per atom in the bulk crystal. In this way, we can explain why

TABLE V. Energy difference between Ih and TO with same size for the surface energy gain and core energy loss divided by the total number of atoms (13, 561, 2057).

| Metal | 13 (surf.) | 13 (core) | 561 (surf.) | 561 (core) | 2057 (surf.) | 2057 (core) |
|---|---|---|---|---|---|---|
| Cu | −0.081 | 0.019 | −0.020 | 0.007 | −0.012 | 0.007 |
| Ag | −0.067 | 0.017 | −0.014 | 0.006 | −0.009 | 0.007 |
| Au | −0.053 | 0.030 | −0.005 | 0.006 | −0.002 | 0.007 |

Cu has a wide size interval in which noncrystalline structures are favored while Au presents a very small crossover size interval. In fact, we find that $\rho(\epsilon)$ depends only on the product $pq$: a large $pq$ (as happens for gold) suggests a sticky potential, so displacing atoms in noncrystalline positions costs a lot. On the other hand, small $pq$ allows to displace interatomic distances and so the icosahedral and decahedral motifs are favored up to large sizes. Therefore, we can conclude that there is a simple way to determine the general trends in crossover sizes among different structures: a crystal which increases strongly its energy for a change in interatomic distances would have small crossover sizes while elements with less sticky interactions would have larger crossover sizes.

## ACKNOWLEDGMENTS

The authors acknowledge financial support from the Italian MURST under project No. 9902112831. We thank A. F. Voter for permitting us to use his Molecular Dynamics code. The CRMC2 is associated to the Universities of Aix-Marseille II and III.

## APPENDIX: FORMULA FOR $\rho(\epsilon)$ WITH SECOND-NEIGHBOR INTERACTIONS

Here we report the results for $\rho(\epsilon)$ in the case of interactions extended to the second neighbors for RGL potentials [see Eqs. (1) and (2) with $\alpha=1/2$]. Following the same procedure as in Sec. IV, one finds easily that $\rho(\epsilon)$ can be cast in the form $\rho(\epsilon)=f(p,q)\epsilon^2$ where $f(p,q)$ is given by

$$f(p,q)=\frac{pq}{2}\,\frac{p\,\dfrac{1+C}{1+\sqrt{2}C}-q\,\dfrac{1-(3-\sqrt{2})D+\dfrac{D^2}{2}}{\left(1+\dfrac{D}{2}\right)\left(1+\dfrac{D}{\sqrt{2}}\right)}}{p\,\dfrac{1+\dfrac{D}{2}}{1+\dfrac{D}{\sqrt{2}}}-q\,\dfrac{1+\dfrac{C}{2}}{1+\sqrt{2}C}}, \qquad \text{(A1)}$$

where

$$C=\exp[-p(\sqrt{2}-1)], \quad D=\exp[-2q(\sqrt{2}-1)]. \qquad \text{(A2)}$$

As seen in Table III the corrections to the first-neighbor result are in between 3–10%. They are larger for Cu and smaller for Au; this follows from the fact that the potential for Cu has the longest range (i.e., it is the least sticky) among the five metals, and the potential for gold has the shortest range. The result with first-neighbor interactions $[f(p,q)=pq/2]$ is recovered by putting $C=0$ and $D=0$ in the above formula.

[1] T. P. Martin, Phys. Rep. **273**, 199 (1996).
[2] L. D. Marks, Rep. Prog. Phys. **57**, 603 (1994).
[3] C. L. Cleveland, U. Landman, T. G. Schaaff, M. N. Shafigullin, P. W. Stephans, and R. L. Whetten, Phys. Rev. Lett. **79**, 1873 (1997).
[4] S. Ino, J. Phys. Soc. Jpn. **27**, 941 (1969).
[5] L. D. Marks, J. Cryst. Growth **61**, 556 (1984).
[6] B. Raoult, J. Farges, M. F. De Feraudy, and G. Torchet, Philos. Mag. B **60**, 881 (1989).
[7] C. L. Cleveland and U. Landman, J. Chem. Phys. **94**, 7376 (1991).
[8] J. Upperbrink and D. J. Wales, J. Chem. Phys. **96**, 8520 (1992).
[9] J. P. K. Doye, M. A. Miller, and D. J. Wales, J. Chem. Phys. **111**, 8417 (1999).
[10] D. Reinhard, B. D. Hall, P. Berthoud, S. Valkealahti, and R. Monot, Phys. Rev. Lett. **79**, 1459 (1997).
[11] J. Farges, M. F. De Feraudy, B. Raoult, and G. Torchet, Surf. Sci. **106**, 95 (1981).
[12] C. Mottet, G. Trèglia, and B. Legrand, Surf. Sci. **383**, L719 (1997).
[13] C. Barreteau, M. C. Desjonquères, and D. Spanjaard, Eur. Phys. J. D **11**, 395 (2000).
[14] V. Rosato, M. Guillopé, and B. Legrand, Philos. Mag. A **59**, 321 (1989).
[15] F. Cleri and V. Rosato, Phys. Rev. B **48**, 22 (1993).
[16] S. M. Foiles, M. I. Baskes, and M. S. Daw, Phys. Rev. B **33**, 7983 (1986).
[17] A. F. Voter, Los Alamos Unclassified Technical Report No. LA-UR 93-3901, 1993.
[18] C. L. Liu, J. M. Cohen, J. B. Adams, and A. F. Voter, Surf. Sci. **253**, 334 (1991).
[19] J. Guevara, A. M. Llois, and M. Weissmann, Phys. Rev. B **52**, 11509 (1995).
[20] F. Montalenti and R. Ferrando, Phys. Rev. B **59**, 5881 (1999).
[21] R. Ferrando, Phys. Rev. Lett. **76**, 4195 (1996).
[22] F. Montalenti and R. Ferrando, Phys. Rev. Lett. **82**, 1498 (1999).
[23] F. Baletto, C. Mottet, and R. Ferrando, Phys. Rev. Lett. **84**, 5544 (2000).
[24] F. Baletto, C. Mottet, and R. Ferrando, Phys. Rev. B **63**, 155408 (2001).
[25] D. Reinhard, B. D. Hall, D. Ugarte, and R. Monot, Phys. Rev. B **55**, 7868 (1997).
[26] K. Michaelian, N. Rendón, and I. L. Garzon, Phys. Rev. B **60**, 2000 (1999).
[27] J. P. K. Doye and D. J. Wales, New J. Chem. **22**, 733 (1998).
[28] A. Pimpinelli and J. Villain, *Physics of Crystal Growth* (Cambridge University Press, Cambridge, 1998).
[29] M. Guillopé and B. Legrand, Surf. Sci. **215**, 577 (1989).
[30] J. H. Rose, J. R. Smith, and J. Ferrante, Phys. Rev. B **28**, 1835 (1983).
[31] D. Spanjaard and M. C. Desjonqures, Phys. Rev. B **30**, 4822 (1984).
[32] J. P. K. Doye, D. J. Wales, and R. S. Berry, J. Chem. Phys. **103**, 4234 (1995).